sustainability

MDPI

Article

Rapid Simulation of Optimally Responsive Façade during Schematic Design Phases: Use of a New Hybrid Metaheuristic Algorithm

Hwang Yi [1,*], Mi-Jin Kim [1], Yuri Kim [1], Sun-Sook Kim [2] and Kyu-In Lee [2]

[1] Architectural Design & Technology Lab, Department of Architecture, Ajou University, Suwon 16499, Korea; askhow1999@ajou.ac.kr (M.-J.K.); archiyuri@nate.com (Y.K.)

[2] Department of Architecture, College of Engineering, Ajou University, Suwon 16499, Korea; kss@ajou.ac.kr (S.-S.K.); kyuinlee@ajou.ac.kr (K.-I.L.)

* Correspondence: hwy@ajou.ac.kr; Tel.: +82-31-219-2493

Received: 3 April 2019; Accepted: 6 May 2019; Published: 10 May 2019

Abstract: Operation of environmentally responsive building components requires rapid prediction of the optimal adaptation of geometric shapes and positions, and such responsive configuration needs to be identified during the design process as early as possible. However, building simulation practices to characterize optimized shapes of various geometric design candidates are limited by complex simulation procedures, slow optimization, and lack of site information. This study suggests a practical approach to the design of responsive building façades by integrating on-site sensors, building performance simulation (BPS), machine-learning, and 3D geometry modeling on a unified design interface. To this end, a novel and efficient hybrid optimization algorithm, tabu-based adaptive pattern search simulated annealing (T-APSSA), was developed and integrated with wireless sensor data communication (using nRF24L01 and ESP8266 WiFi modules) on a parametric visual programming language (VPL) interface Rhino Grasshopper (0.9.0076, McNeel, Seattle, USA). The effectiveness of T-APSSA for early-stage BPS and optimal design is compared with other metaheuristic algorithms, and the proposed framework is validated by experimental optimal envelope (window shading) designs for single (daylight) and multiple (daylight and energy) objectives. Test results demonstrate the improved efficiency of T-APSSA in calculations (two to four times faster than other algorithms). This T-APSSA-integrated sensor-enabled design optimization practice supports rapid BPS and digital prototyping of responsive building façade design.

Keywords: design optimization; optimization algorithm; adaptive building façade; building performance simulation

1. Introduction

Many in the discipline of architecture have long envisioned buildings that, against their inherent immobility, interactively respond to ambient contexts [1–3]. On the strength of a host of emerging technologies, such as smart materials, 3D printing, artificial intelligence, and the internet-of-things (IoT), making buildings physically interactive is no longer an act of the imagination; responsive or kinetic buildings have already been realized in the Al-Bahar Towers and Korean Pavilion EXPO 2012 [4,5]. As newer computational media and biotechnologies transform building design and construction, a number of experimental studies are exhibiting innovative, interdisciplinary methods for design and fabrication [6–9].

Heightened interests in movable types of buildings closely pertain to a growing need for an architectural responsibility for environmental sustainability. Active engagements with buildings, through dynamic settings and bioclimatic adaptations of geometrical shapes in natural and human

environments, are valued for improving indoor thermal comfort and operational efficiency by mitigating energy consumption and carbon emissions, without an additional use of fuel or the installation of equipment [10,11].

To make responsive buildings more environmentally effective, a prudent understanding of the dynamics of building performance is necessary from the opening stage of a project; both the design of morphological variation and control strategies of motional parts need to be carefully tested and predicted while exploring design candidates. Well-planned building kinematics will be concerned not only with a formal aesthetic quality, but also the capability of making instant and precise environmental interventions between interiors and exteriors in rapidly changing building contexts.

However, practice for the simultaneous identification of design quality and the environmental effectiveness of moving parts is still nascent and the best method has yet to be known especially in the schematic stages of building projects. Existing design tools and building performance simulation (BPS) are insufficient to support dynamic design and the simulation of responsive mechanism. Despite many studies on the simulation-deployed design process using building information modeling (BIM) [12], BIM and BPS tools carry limited capacity to interface the environmental analysis of responsive building form with the architectural design process. BPS engines are primarily targeted at building engineers less concerned with building geometry than mechanical systems, and simulation algorithms set a limit on associating energetic feedback from dynamic formal change with design outcomes. Moreover, lack of actual information on building contexts in BIM and BPS, specifically in the early phases of environmental building design, quite often result in incomplete performance validation, leaving design decisions with a lot of uncertainty [13]. Also, there is a dearth of research on how to test the optimal controllability and performance of responsive operation during the design process. Optimization methodologies for building design and software add-ons to support geometry optimization (e.g., Goat or Galapagos for Rhino) focus on finding deterministic solutions of rigidly finalized forms, and occasionally sluggish convergence of genetic algorithm (GA) and simulated annealing (SA) in design search may significantly delay the process of obtaining design outcomes [14,15].

This study aims to fill these knowledge gaps in early-stage optimal responsive design, addressing a practical (designer-oriented) approach built on the integration of BPS, optimization algorithms, and electronic sensors with parametric building modeling (Figure 1). A visual programming language (VPL) using Python (IPython)in Rhino Grasshopper (GH) is used to implement software procedure, as well as hardware-sourced data, through a unified graphical design interface (GDI). For the sensor-triggered optimization of responsively operational patterns of façade form, metaheuristic algorithms are hybridized to quicken the iterative solution search. A hybrid direct search algorithm incorporating the advantages of existing metaheuristic is proposed for this study and referred to as tabu-based adaptive pattern search SA (T-APSSA). The objective of this research is to demonstrate the efficiency of T-APSSA for rapid and dynamic design decision-making, and it is tested on a GDI for schematic façade design.

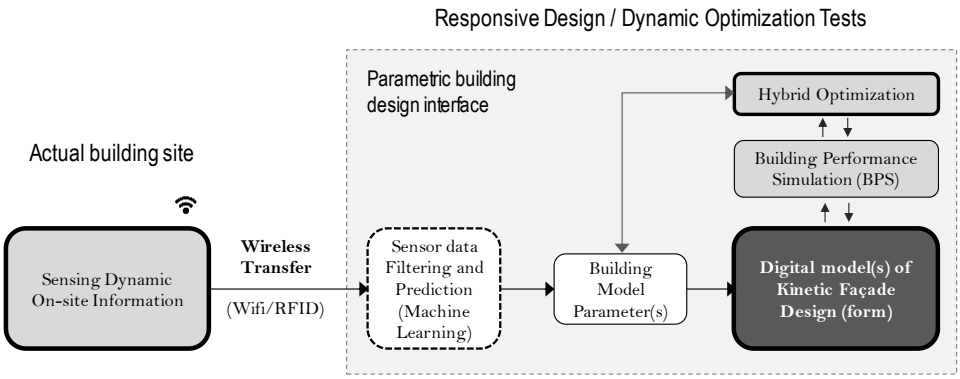

Figure 1. Test scheme of the sensing-triggered early-stage responsive façade design optimization: Use of Wi-Fi and Radio-frequency identification (RFID) for the design workspace.

2. Related Work: Responsive Façade Design, Parametric Automation, and Optimization

2.1. Responsive Façade Design for Sustainable Architecture

Responsive building design is a subject within the broad domain of environmentally adaptive architecture, also known as interactive or kinetic architecture. While responsive building interaction can be addressed at different levels, such as shape, manufacturing, process, and functioning with various systemic principles [8,16], responsive building kinematics take mechanistic forces and principles of motion to change the size, form, or composition of a whole building or its parts. Its basic concepts and terminology were introduced in the 1970s [17], but along with the rise of the green building industry, the adaptively movable building is once again gaining increasing popularity as an emerging paradigm in sustainable architecture and building design education. Lee et al. [11] suggested simplified formulas to estimate the energy performance of movable windows, and Yi [18] discussed robotics-based design experiments as well as the educational effectiveness of introducing kinematics into design studio curriculums. In particular, the responsively acclimatized design of building enclosures, inspired by biomimicry (or biomimetics) that takes the characteristics of nature as a dominant driver for design strategies and form-making [5,9,19], is progressively studied with a high-level abstraction of natural principles, owing to the development of robotics and sensor technologies [8]. Nevertheless, despite many conceptual projects and methodological proposals regarding building responsiveness [6,7,9,19], the problem of how to incorporate environmental simulations of the motions of building parts is addressed less in the context of early design processes. This is mainly because (1) the existing tools are technically insufficient to support the complex design of dynamic building motion [12]; (2) it is difficult to develop a mathematical simulation algorithm that is generally applicable to the diagnosis of responsive building performance [11]; and (3) there is a lack of a standardized procedure or protocol regarding the automation and optimization of adaptively moving geometry [5,9].

2.2. Problems in BPS for Early-Phase Responsive Design Validation

The emerging digital tools integrating BIM, 3D visualization, automation, and BPS have enabled architects and engineers to process a great deal of building data during design phases [20,21]. In conjunction with increasing awareness of building sustainability, the development of easy-to-use building design interfaces, and cheap computational platforms supporting BPS, data processing algorithms, optimization, and/or parametric form generation, are accelerating the wide spread of environmental information-driven form-making or performance-based design in the practice of architecture [20,22–24].

Geometrically responsive types of environmental buildings supported by these instruments are often delivered with complicated building shapes [4], in which, in particular, movable parts cause an increase in complexity, inputs, and cost of construction. Thus, the practical application of responsive building ideas must allow for closer examination, from the beginning of building projects, of the effectiveness and technical merits of formal variations toward the improvement of building performance. Design decisions for sustainably adaptive geometry should be fully simulated throughout the process and informed by responsive components and interactively changing building performances (energy use, indoor comfort, etc.). However, the dynamic BPS of kinetic buildings has not been fully elucidated and incorporated in terms of design practice, due to the limitation of existing algorithms and obscurity of the process. For example, EnergyPlus (EP) (National Renewable Energy Laboratory, USA) offers a behavior-interactive energy simulation module, an energy management system, and a third-party middleware with simulation-wrapping algorithms such as the functional mock-up interface and the building controls virtual test bed, which enable interactive co-simulation. Unfortunately, implementation of these methods to the design of adaptive building geometry is significantly limited, as they account primarily for non-geometric building variables (e.g., window shading area, occupancy schedule, or thermostat set points). Lee et al. [11] suggest a numerical algorithm to simulate the energy use of an external kinetic shading system, yet it means little to the

practice of early-phase decision-making, which involves commercial design software and the informal shapes of kinetic components. BPS plug-ins for digital design tools (Insight 360 for Revit, DIVA for GH, etc.), which are widely used among architects, also expose a fundamental limitation, as their performance simulation implements as-is existing engines (EP, Radiance, etc.) and nonlinear building designs, such as non-uniform rational basis spline geometry, that are not completely supported. On the other hand, responsive building operation depends on real-time changes of interior/exterior building environments, and BPS-optimization coupling for responsive building design requires actual building data. Fueling the BPS process with accurate site/building information reduces the uncertainty of performance results; however, little attention to the early validation of responsive design has been called for. The difficulty of collecting precise data on local weather or a building site and limited BPS support for complex geometry, are dominant factors that obstruct rigorous performance tests of building interaction.

Recently, the rapid spread of sensor and mobile technologies to the architecture, engineering, and construction (AEC) industry are advancing 3D BIM to the 4D/*n*D paradigm coupled with a simultaneous real-time coordinate [21]. However, in the environmental building design process, the integration of dynamic information from the real-world and BIM-BPS has not yet been fully highlighted [12,22]. A key to bringing more actualities and accuracies to BPS and design is unfolding the standalone working of a single-purpose simulation, thereby coupling it with real-world parameters, so as to strengthen the responsive mechanism between the digital environment and actual representation. This concern raises cross-disciplinary technical issues, such as tether-free data communication, sensing of physical systems, remote visualization, and self-adjustment in data transmission.

2.3. A Need for Rapid Optimization Methods in the Early-Stage Simulation of a Moving Pattern of Adaptive Building Geometry

Environmental responsive buildings assume dynamic operational mechanisms that are optimized to indoor thermal comfort and energy efficiency. Accordingly, in terms of building form design, it is important to identify how morphological variations guarantee optimal building operation in terms of both building aesthetics and performance. Although optimization-embedded approaches to environmental building design help to find better architectural solutions with formal prototyping [20,25,26], they entail two major problems: (1) static optimization that is little-concerned with time-dependent variables; and (2) laggardness of solution search activities [23]. In most cases, while design optimization focuses upon suggesting a static (non-responsive) design solution for building shape, space arrangement, and indoor settings [20,22,23], optimization of dynamic formal variation is hardly taken into consideration. Moreover, BPS-coupled design optimization is computationally intensive, and may delay the design process as heuristic algorithms run hundreds of simulations [25,26]; it takes a few minutes to hours to converge the exhausting architectural feedback. There can be three methods to resolve this issue: (1) reduction of model/variable complexity; (2) reframing the search procedure with simpler sub- or dual-problems [27,28]; and (3) meta-simulation using statistical approximation [29]. However, simplification of building modeling is not feasible when architectural design lays stress on the visualized representation of form, as loss of architectural details in BIM for BPS-optimization occurs. Subdividing an optimization problem into several sub-problems (e.g., hierarchical processes) or dual representations can be a good option, but there exist few general procedures that are applicable to all building problems. Unsuccessful convergence in local problems may cause failure in global search. Employment of a simplified surrogate of BPS using statistical techniques (e.g., black box simulation) needs a lot of prior simulation runs and post-processing (e.g., uncertainty and sensitivity analysis) to establish a valid meta-model.

Therefore, an alternative robust search algorithm specific to responsive design needs to be developed to handle dynamic data quickly, and the hybridization of existing algorithms can be an idea. However, the selection and customization of known algorithms needs to be done carefully, as each has its pros and cons. Due to the complexity and high-dimensionality of cost functions and constraints,

the majority of design optimization rests upon metaheuristic techniques, such as SA, pattern search (PS, also known as direct search), and GAs or EAs. GAs are most widely used for building problems, and have been found to be well-suited to multi-objective optimization (MOO) [14,20,26]. Nevertheless, they do not always ensure high-quality solutions as they need some expert skills to predetermine design operators, and the success of a search depends highly on a set of complex refinement rules and stochastic parameters regarding the sampling method of individuals, genetic diversity of population (crossover and the probability of mutation), and elitism (selection of the fittest candidates) [30]. In practice, convergence in GAs can also be significantly delayed or might even fail if the number of variables increases, because binary (or decimal) encodings of real values may cause search space size to exponentially grow. More critically, GAs are limited to operating on dynamic datasets, because evolution strategies often deterministically converge toward local minima before follow up data are available [30,31]. Meanwhile, SA explicitly (rather than working with a group of feasible solutions) searches for a global optimum with a far simpler operation; non-reduction of variable complexity prevents ill-mapping of a global search domain [32]. Although SA is intuitively programmable and flexibly implementable, longer search times to reach a global solution in continuous domains are ill-suited to problems with time-dependent variables. Global search methods including GAs and SA employ stochastic operators to sacrifice short-term fitness to gain global optima, which makes the search process vulnerable to parameter change, delaying the process. To reduce convergence time, we can diminish a variable domain into non-continuous space, since geometry variables in building problems can be converted to domain-specific discrete numbers that are not very sensitive to minute number change. In this context, implement of PS offers rapid solutions for building problems, as a fewer number of iterations are necessary. PS significantly reduces time complexity, as the PS heuristic explores only feasible candidates through discretization of a continuous variable domain (grid mesh). PS is thus found to be effective for local searches as well as global optimization [33]. That said, it is too sensitive for mesh definitions, and unsuitable choices of the mesh parameter (mesh size) tend to end up with local optima [34]. This can be overcome by integrating a global method or tabu search (TS) [35,36]. For this reason, this study attempts to hybridize the advantages of SA, PS, and TS to develop a novel fast search method. Section 3.3 demonstrates the effectiveness of this method for BPS and design optimization.

3. Proposed Method

3.1. Test Building Site and Design

The proposed framework is applied to the test design of a responsive façade (window shading design) for optimal indoor daylighting. External shading devices are an important component of building envelope design that largely impacts daylight use and air conditioning, particularly in hot climates. Due to this significance, optimal shading design and daylight control have been dominant topics in building design optimization [7,11,37,38]. The test building was part of an architecture school complex at Florida International University (FIU), located in southwest Miami, Florida. The redesign target was the fixed double-glazing façade of an interdisciplinary facility, the Structural and Environmental Technologies Lab (FIU-SETLab), which is dedicated to the teaching and research of sustainable architecture (Figure 2). The SETLab façade faces a large east courtyard and is exposed to a significant amount of sunlight and radiance. This space suffers from overheating and glare during daytime. To integrate parametric design and BPS into GH, DIVA—a Radiance-based lighting simulation plug-in—was selected to design and simulate the indoor daylight level due to the façade's design. The sky illuminance in Radiance was pre-set according to static sky model types (sunny, clear, overcast), or by using the Perez sky model, which imports historic weather records of a local area that are neither dynamic nor site-specific. Daylight simulation can become more realistic and precise by importing the actual solar radiation data of a weather file to construct a customized sky model (Figure 3). The as-is simulation results in Figure 3 show that indoor daylight levels depended

highly on the input sky models. In this study, the actual weather information read from light sensors installed at the site are integrated into GH and DIVA.

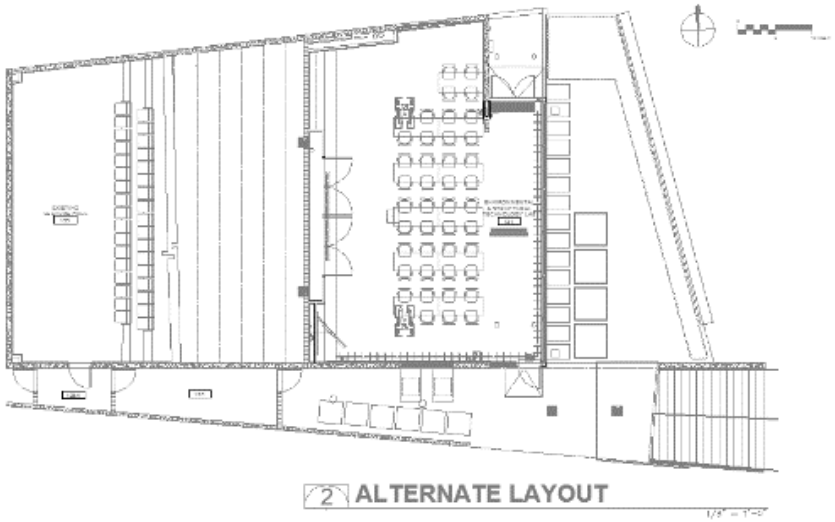

(**a**)

(**b**)

(**c**)

Figure 2. Test building (Florida International University, Miami, FL, USA). Note: (**a**) plan; (**b**) front view with the court yard; (**c**) interior view.

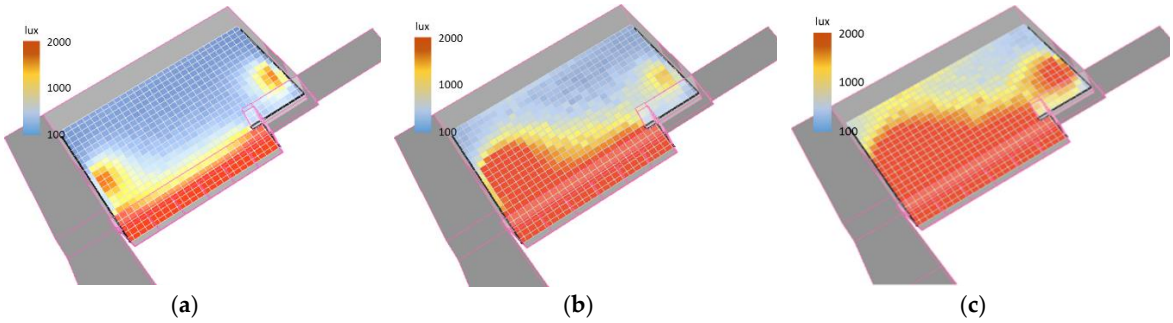

Figure 3. Geometric modeling of the test building and test results of radiance daylight simulation under different sky models. Lux measured from an on-site photoresistor was converted to solar radiation (W/m^2) using a daylight luminous efficacy factor (EF) of 121.5 lm/W [39]. (**a**) Overcast sky model. (**b**) Customized sky model with on-site actual data (1:15 p.m., 15 February 2017). (**c**) Customized sky model with on-site actual data (1:19 p.m., 15 February 2017).

3.2. Preliminary Sensor Tests and Hardware Installations for Data Transfer

A major task of this study was to integrate on-site measuring hardware with a designer's workstation. However, there are few portable irradiance sensors available for laptops; solar radiation is thus measured indirectly by converting illuminance values. To measure outdoor luminosity, a TSL2591 digital sensor was prepared, as it is a high-precision device for microcontrollers with the widest range of detection (0–80,000 lux) and the greatest sensitivity (188 lux). Nevertheless, bright sunlight measures greater than 100,000 lux. A standalone precision sensor (LX1330B; measuring 0–200,000 lux; <±1% error rate in 0–40 °C) was thus used to cover the full range of solar luminosity. Meter readings from the TSL2591 were converted to actual values of the LX1330B (Figure 4).

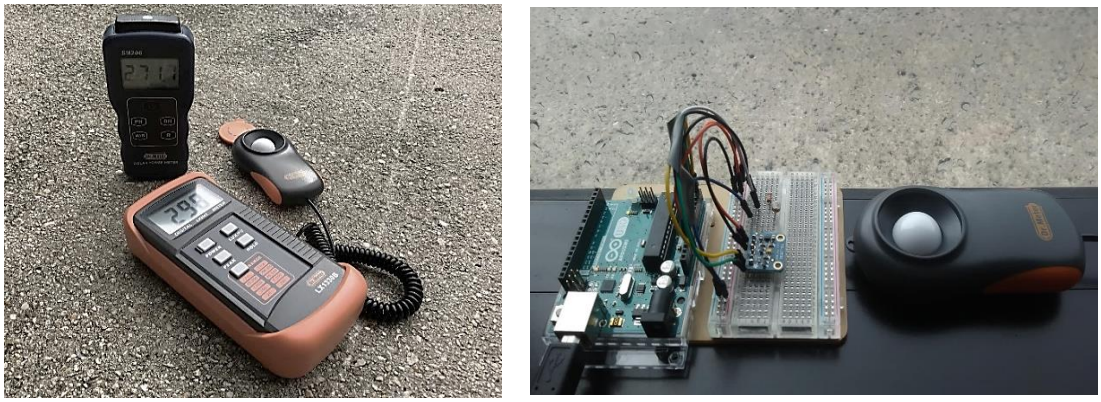

Figure 4. Preliminary field tests of sensors for fault detection. (**a**) An illuminance meter (LX1330B) and a solar radiation sensor (SM206). (**b**) Digital light sensor (TSL 2591) validation.

Installing the equipment on a horizontal ground in front of the test building, preliminary field tests were conducted to identify different measurements of the sensors and correct their readings. Solar radiation is interchangeable with luminosity through a luminous efficacy (LE) conversion factor. To evaluate LE around the site, an SM206 sensor (range:0.1–399.9 W/m^2; 0.1 W/m^2 resolution with ±3% accuracy in 0–50 °C) was used to gage solar radiation. As shown in Figure 4a–c, solar illuminance and irradiance were measured on the same horizontal plane every two minutes between 2:00 and 3:00 p.m. (the hottest hours in Miami) from 14–18 August 2017 (mostly clear and sunny sky, 12~25% clouds) at the site, with 150 data collected. The daylight efficacy factor (EF) is known to be around 100 lm/W or greater in a tropical hot climate [39]. An average EF at the site similarly measured 108.6 lm/W, and Figure 5 shows that the irradiance was linearly proportional to the illuminance, with an R-square value of 99.5% (luminosity readings are easily convertible to radiation values using a linear regression

model). Readings between the TSL2591 and LX1330B were linear at lower light levels but exhibited an overall inconsistency due to their different sensitivities under the spectrum of light intensity (Figure 5).

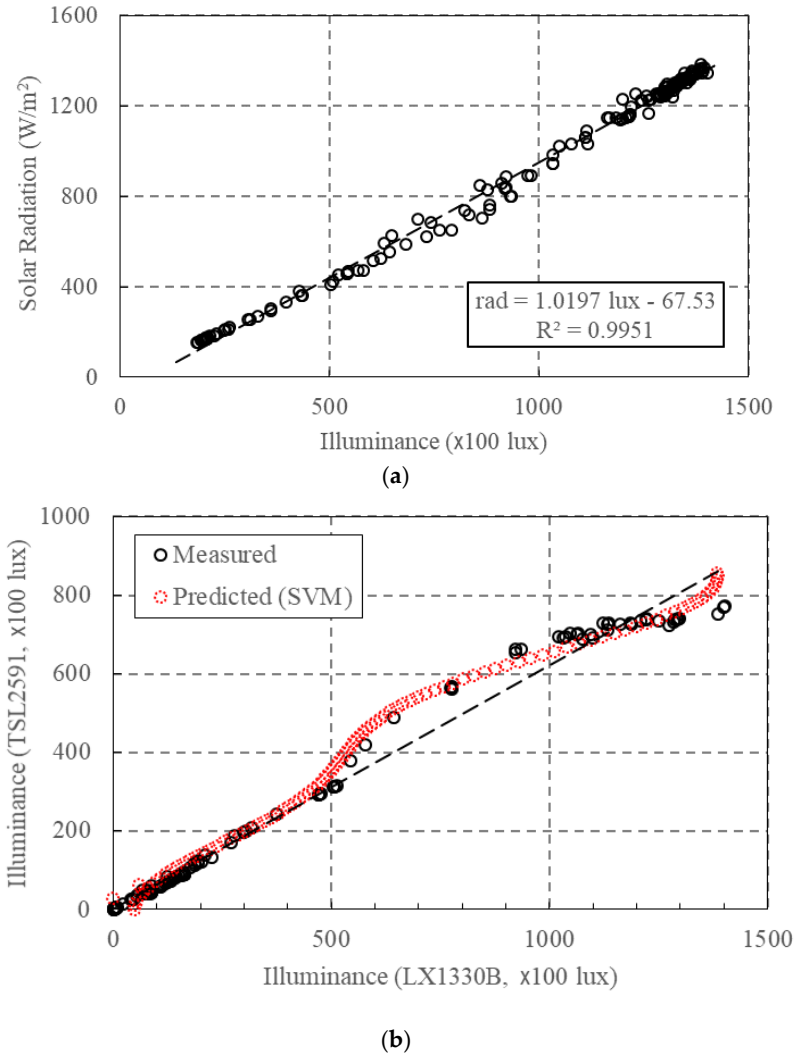

Figure 5. Training sets of sensor data and identification of relationships for data correction. (**a**) Training data for SVM modeling. (**b**) Comparison of SVM predictions and actual data.

To convert the TSL2591 readings to the more realistic ones of the LX1300B, a prediction model using a support vector machine (SVM) was identified (Figure 5). SVM offers an efficient learning algorithm for complex regression analysis. The developed SVM model encoded in IronPython was implemented in the GH design interface, so that on-site readings from the TSL2591 approximated the precise luminosity and irradiation used to construct a realistic sky model for a dynamic daylight simulation. The tested light senor was integrated into an Arduino microcontroller, and the complete instrument was combined with a WiFi shield (ESP8266). A radio-frequency (RF) radio transmitter (nRF24L01) was installed in the test building site.

3.3. Hybridization of Optimization Algorithms: Tabu-based Adaptive Pattern Search Simulated Annealing (T-APSSA)

Given a solution domain Ω, the goal of T-APSSA is to find an optimal value of x' to minimize the cost function:

$$f_\Omega(x), \text{ i.e., } x' = arg\ \min f_\Omega(x), \forall x \in \Omega, f\colon \mathbb{R} \to \mathbb{R} \cup \{\infty\}. \quad (1)$$

In the algorithm, a series of hybrid operation parameters are chosen, such as a step index $i \in \mathbb{N}_0$, an initial and loop termination temperature (T_0 and T_{min}), and an annealing schedule factor ($\alpha \in (0,1)$, a ratio of temperature degradation) from the SA heuristic; ξ denotes the memory size of a tabu list (TL) containing visited vectors. A solution is expressed as point vector $\boldsymbol{x}$ such that

$$\boldsymbol{x}^{\theta} = \{x^{\theta}{}_{ik}\},\ \theta = 1, \ldots, n,\ k = 1, \ldots, p, \text{ and } n, p \in \mathbb{N}_1 \tag{2}$$

where $\boldsymbol{x}^{\theta}$ denotes the θ-th trial solution (a set of feasible points), n is a sequence, and k is the number of local points.

This algorithm constructs a loop of SA-based iterations, and at each step candidates are selected based on the PS strategy that subdivides Ω into a k-dimensional set of mesh points. The grid resolution is determined by a mesh size parameter, $\boldsymbol{\Delta}_i \in \mathbb{R}^n$. According to the number of trial points (n), each candidate has an associated neighborhood on the mesh grid, $N_i(x^{\theta}{}_{ik}, \theta = 2, \ldots, n) \subset \Omega$. At the first step, $i = 0$, a feasible vector $\boldsymbol{x}_0$ is set, followed by an initial cost $f(\boldsymbol{x}_0)$. A new trial point, $\boldsymbol{x}^{\theta}{}_i$, is then randomly chosen as an incumbent solution, and generates a neighborhood of mesh vertices (N_i) centered around $\boldsymbol{x}^{\theta}{}_i$, defined as

$$x^{\theta+1}{}_{ik} = x^{\theta}{}_{ik} \pm \boldsymbol{\Delta}_i d_k \tag{3}$$

where $d_k \in [I]$ spans the coordinate axes (a mesh frame).

Per each neighbor, fitness (E) is evaluated, and the best value $\boldsymbol{x}^{\prime\theta}{}_i$ is obtained within the pool of mesh points. Compared to the solution in a previous state of the problem, the Boltzmann formula ($e^{(\text{E-E}new)/\text{T}} > r \in (0,1)$) informs the acceptability of the current value. Stochastic transitions to small downhills prevent the PS from falling into local minima and improve search quality. This heuristic is iterated until the search converges with a global optimum or suits some termination criteria (Figure 6a).

Integration of a mesh adaptive PS (MAPS) and TS approach [35,36] plays a critical role in increasing the efficiency of T-APSSA. Uniform spanning of mesh vertices due to fixed mesh size parameter (Δ) is vulnerable to domain scale change, delaying the convergence time. Flexible modification of the mesh parameter and diversification of the neighbor spanning by dynamically changing Δ and d can quicken the heuristic. To this end, on top of the mesh size parameter, the poll size parameter (Δ^q) is introduced, so that $\Delta_i{}^q = k\sqrt{\Delta_i}$. Δ^q defines the boundary of the stepwise refining of an incumbent solution in a state (Figure 6b), the candidates for which are obtained by

$$\boldsymbol{x}_{\boldsymbol{i}}^{\boldsymbol{\theta+1}} = \boldsymbol{x}_{\boldsymbol{i}}^{\boldsymbol{\theta}} \pm \mu \boldsymbol{\Delta}_{\boldsymbol{i}} \boldsymbol{d} \tag{4}$$

where μ is a random number from $\{\mu \mid 1 \le \mu \le \Delta_i^p / \Delta_i,\ \mu\ \mathbb{N}\}$.

Note that $\Delta_{i+1} = 2\Delta_i$ if the solution is improved, otherwise $\Delta_{i+1} = \Delta_i/2$. Ω is scaled to be [0, 1] for PS, and $x_{ik}^{\theta} = d_k$, if $\Delta_i^p > \Delta_i$, because all neighbors become placed on the domain boundary. If a MAPS transition is successfully executed, a TL stores the optimal value ($\boldsymbol{x}^{\prime\theta}{}_i$) and cost as elements, depending on its memory length $\xi \in \mathbb{N}_1$. When generating a new candidate, $\text{TL} = \left\{t_j\right\}_{j=1}^{\xi}$ is referred, to avoid neighborhood areas once visited (tabu regions; TRs) [35]. TRs are circular areas around $\boldsymbol{t}_j$ with a radius r_{TR}. Given a TL and a new trial point $\boldsymbol{x}^0{}_{i+1}$, new search directions outside TRs (Figure 6b) are overridden by:

$$\lambda\left(\boldsymbol{x}^0{}_{i+1} - \bar{\boldsymbol{t}}\right) \tag{5}$$

where $\bar{\boldsymbol{t}} = (\sum_{j=1}^{\xi} \boldsymbol{t}_j)/\xi$, and $\lambda \in \mathbb{R}$ is a random number greater than $max\{\|\boldsymbol{x}^0{}_i - \boldsymbol{t}_j\|\}_{j=1,\ldots,\xi} + r_{\text{TR}}$.

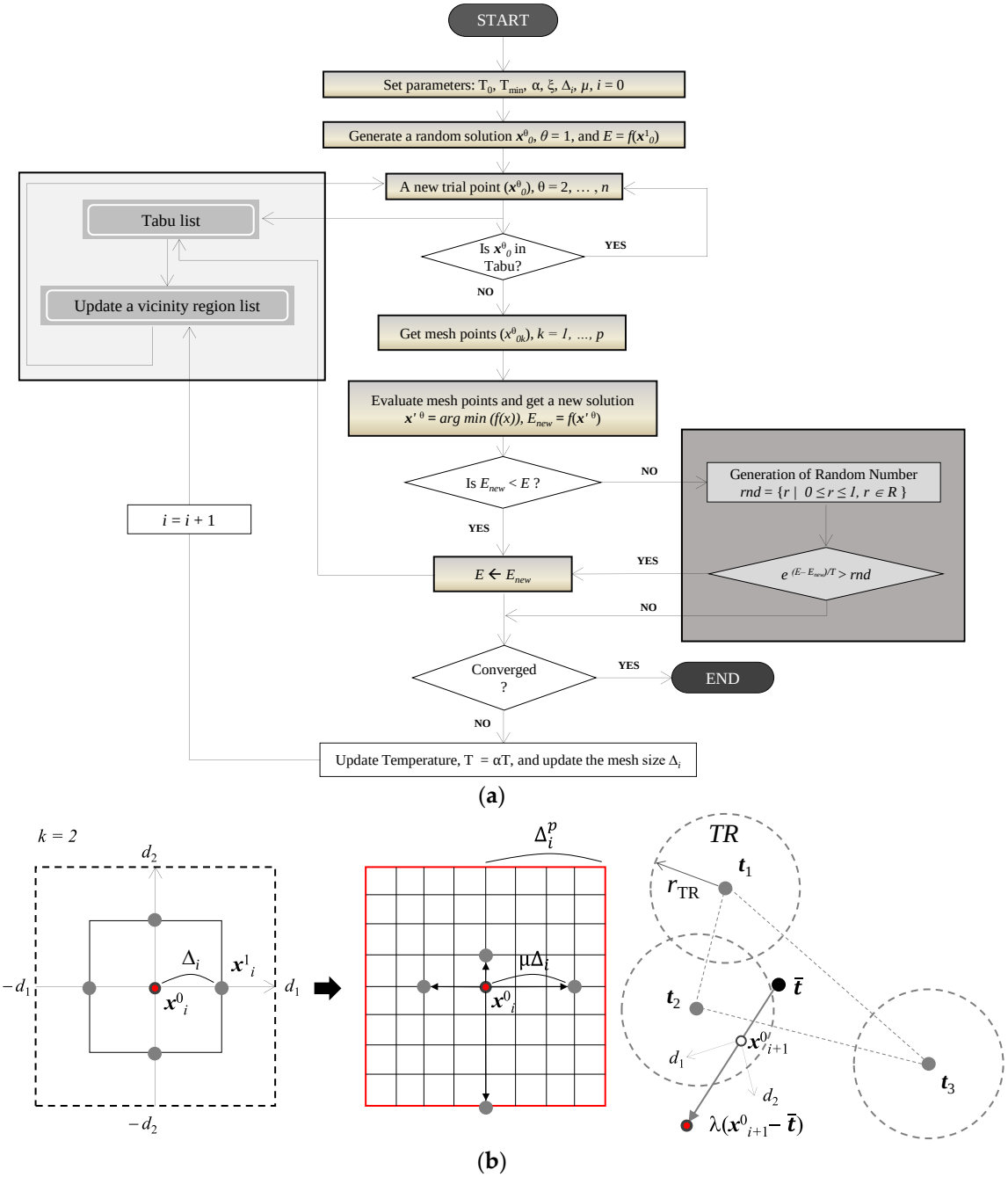

Figure 6. Scheme of T-APSSA. (**a**) Algorithm flow chart. (**b**) Adaptive mesh strategy (left), and a new candidate search from the tabu list (right).

4. Validation of the Method

4.1. Validation of T-APSSA for BPS Practice

The developed hybrid algorithm was coded in GH using Python to seek its practical applicability to early-stage design optimization. To validate the performance improvement of the algorithmic hybridization, the degree of convergence rate and the precision of each optimization algorithm were evaluated with some widely used test functions (Figure 7 and Appendix A). Equations of the cost functions, boundaries of the object variables, and global minima were given accordingly.

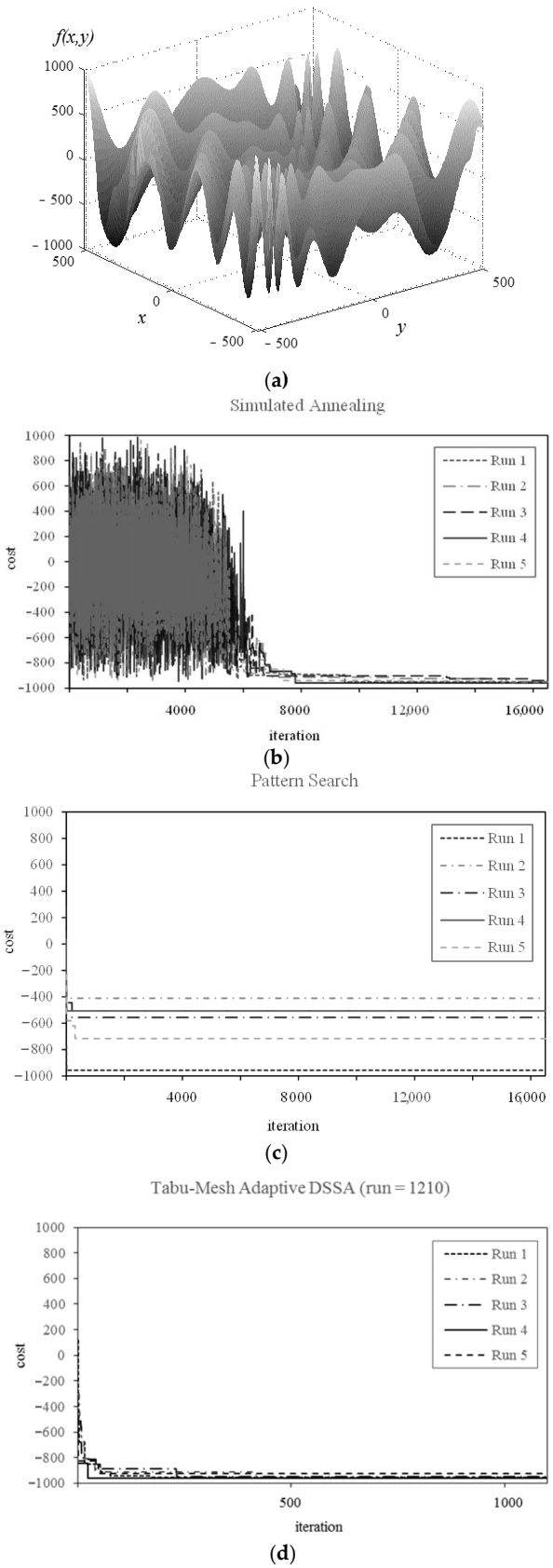

Figure 7. Convergence tests of SA, PS, and T-APSSA with the Eggholder function (upper left). (**a**) Eggholder function; (**b**) simulated annealing; (**c**) pattern search; (**d**) tabu-mesh adaptive DSSA.

Simple performance tests with an artificial landscape (Eggholder function: $f_{\min}(x,y) = -959.6407$, where $-512.0 < x, y < 512.0$) in Figure 7 show quite different characteristics of algorithms. To overcome the PS's tendency to fall easily into a local minimum, a method using a flexible mesh size per each run was suggested as a mesh adaptive direct search (MAPS) [34]. MAPS apparently outperforms PS, but does not completely find global optima, as it is also mesh-dependent (Figure 8). To activate global moves in a direct search, PS or MAPS can be combined with SA so that local minima escape through stochastic transitions, rather than always finding better solutions. The hybridization of PS with SA (PSSA) was suggested with a demonstration of superior performance [36]. The potential of PSSA can be strengthened far more by taking advantage of a set of search rules, such as data logging (tabu direct search; [36]) and mesh adaptivity. At each iteration, a TL contains individual candidates with the best cost, so that discrete random walks will not explore neighborhoods previously visited in a search space. The last result in Figure 8 exhibits the high performance of the mesh adaptive PSSA integrated with TS (memory size = 50). While SA converges after about 12,000 iterations, T-APSSA finds optima at around 200 iterations, which is 6–8 times faster than SA.

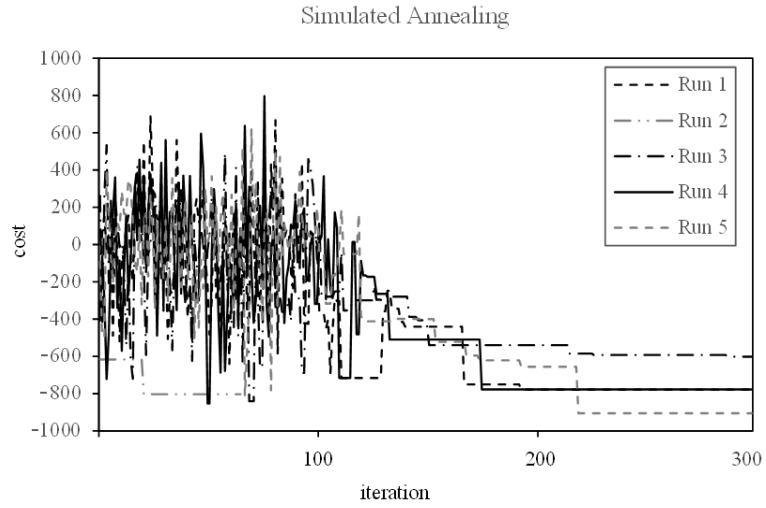

(**a**)

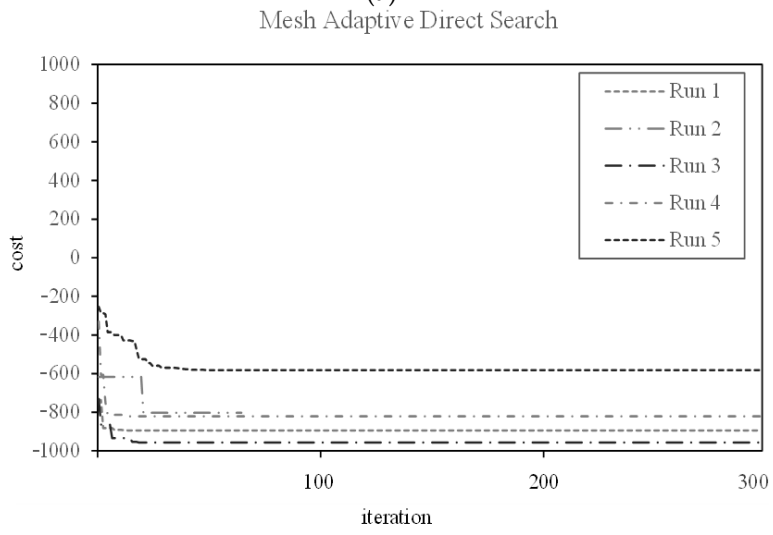

(**b**)

Figure 8. *Cont.*

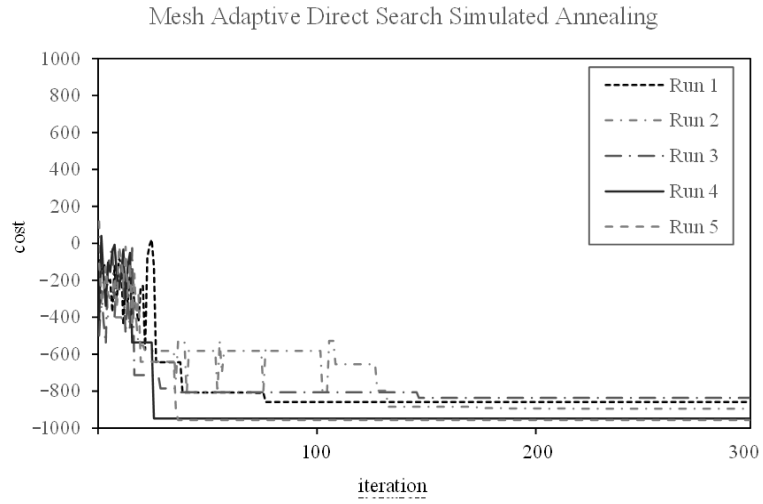

(**c**)

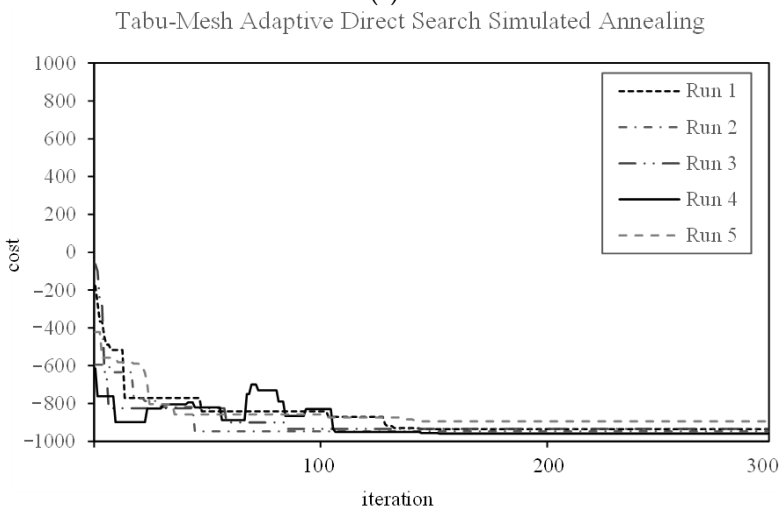

(**d**)

Figure 8. Comparison of optimization performances over 300 iterations. (**a**) simulated annealing; (**b**) mesh-adaptive direct search; (**c**) mesh-adaptive direct search simulated annealing; (**d**) tabu-mesh direct search simulated annealing.

4.2. Encoding T-APSSA into BPS and Test Results

To verify the actual performance of T-APSSA in BPS, T-APSSA and other algorithms were scripted with an architectural BPS tool, Autodesk Ecotect 2015 (Figures 9 and 10). Before this, efficiencies of the algorithms were compared within a limited iteration (300) using the Eggholder function again. The results in Figure 9 show that a mesh adaptive hybrid of PS with SA yields better solutions by escaping local pitfalls with early probabilistic changes, while SA and MAPS hardly converge for the optimal cost. T-APSSA (initial temperature = 50,000 K; termination = 0.001 K; internal iteration = 3; cooling rate: 0.85) reached global optima in 150 iterations. For the performance of the metaheuristics in multi-objective building performance optimization (MOBPO), a simple space volume (Figure 11) was tested with 10 geometrical variables regarding the glazing size and surface area, such as: 2.00 m $\leq wd_{\text{floor}}$, $ln_{\text{floor}} \leq$ 6.00 m, 0.10 $\leq w_{g1}$, h_{g1}, w_{g2}, h_{g2}, w_{g3}, h_{g3}, w_{g4}, $h_{g4} \leq$ 0.90, where wd_{floor} ln_{floor} = 9.00 (m^2), and the ceiling height is 3 m. This test model is assumed to represent a single thermal zone (a room), as simply as possible, with fenestration on each side. To identify influence from the shape change of the envelope, the internal volume of the cubic model remains constant.

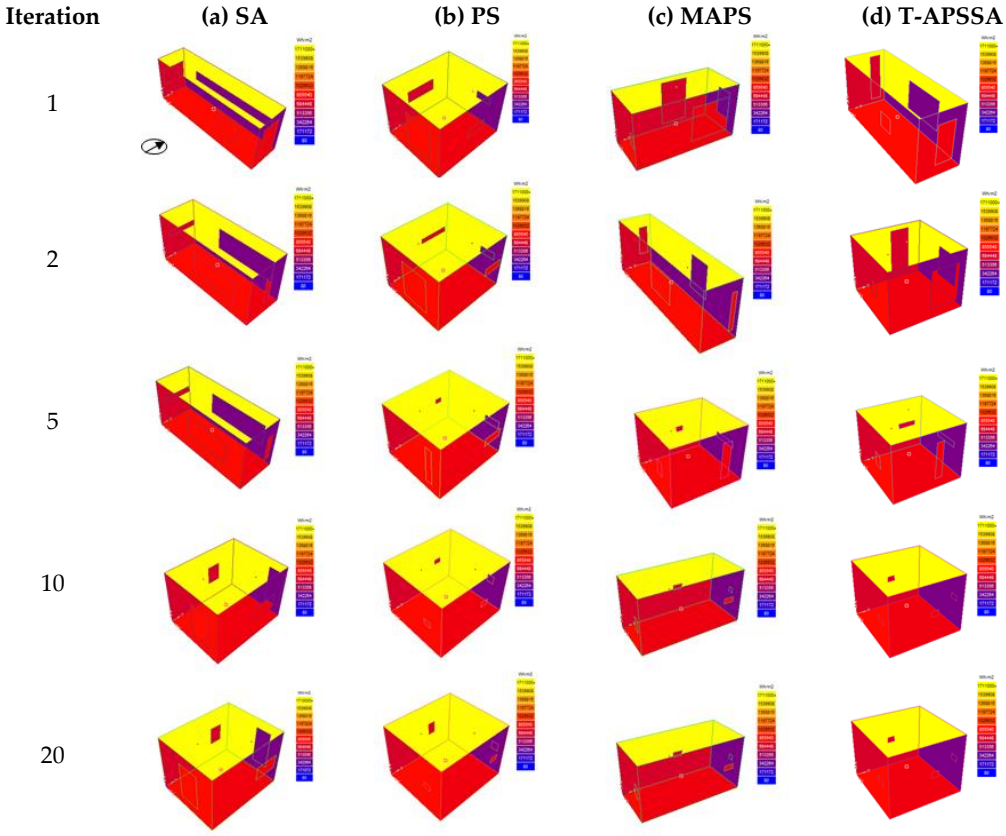

Figure 9. A test model and the results of test 1 for multi-objective building performance optimization (energy and irradiance).

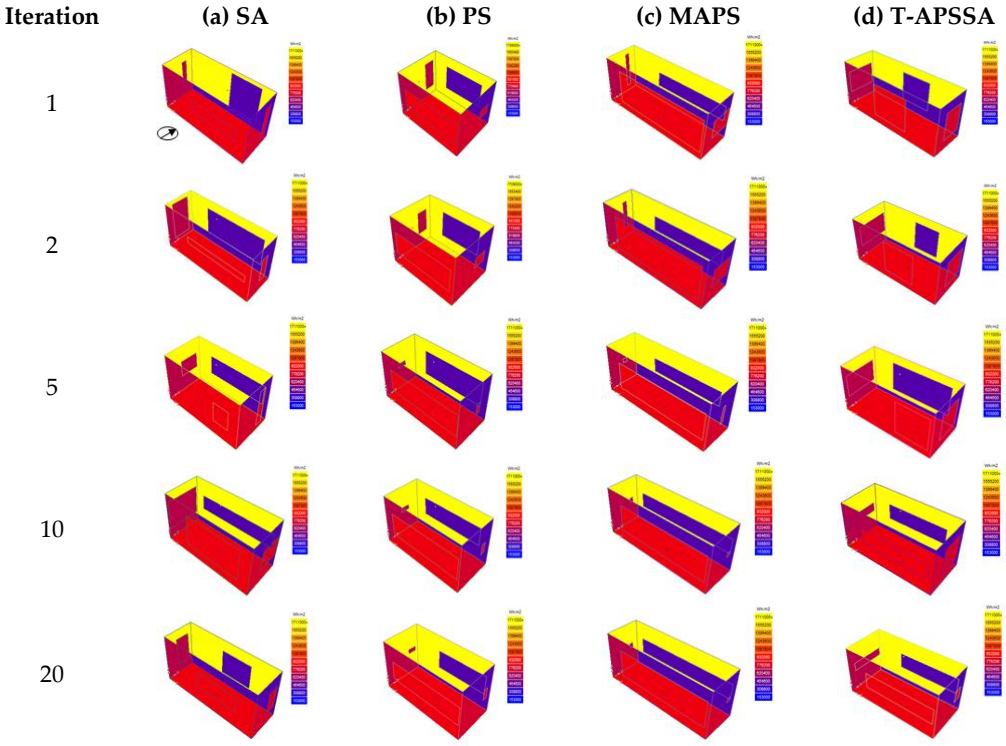

Figure 10. Multi-objective building performance optimization test 2 (energy, irradiance, and daylight).

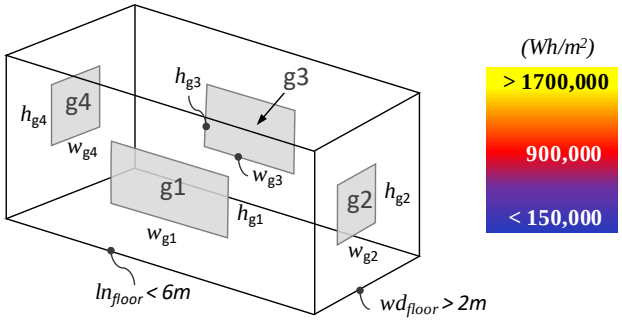

Figure 11. Optimization test model configuration.

The goal of this experiment was to characterize the behavior of the algorithms within a limited number of only 20 iterations. The first MOBPO was tested with the geometric constraints of the Miami climate, to determine an optimal form minimizing both annual end-energy use and surface irradiance with the same weight (Figure 9). Although solar radiation over surfaces is a dominant part of energy loads in hot climates, a minimal energy form needs to orchestrate differently oriented surface areas and windows. In Figure 9, the best building form tended to minimize both envelope surfaces (especially south-facing) and window area to avoid overheating. The test results revealed that SA performed worse than others, while PS and T-APSSA converged very quickly. MAPS was also better than SA, but in this case, mesh adaptivity degraded the search quality. In this test, we identified that, for a simple convex function with a limited number of variables, flexible stochastic moves prevent rapid convergence, and this weakness can be offset by memorizing search traces (Figure 12a). Secondly, to test a more complex MOBPO case, conflicting performance goals were set with the same variables and constraints—minimizing energy use and surface radiation, while maximizing interior daylight (Figure 12b).

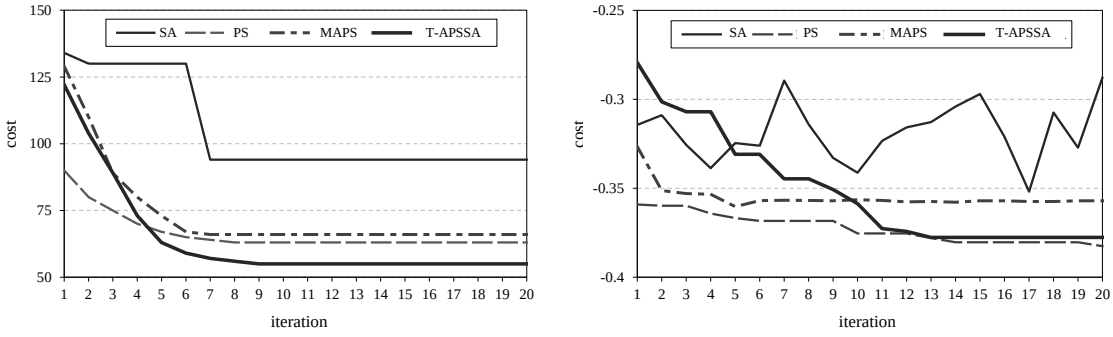

(**a**) (**b**)

Figure 12. Comparison of algorithm performance. (**a**) Cost (MWh): energy + irradiation. (**b**) Cost (scaled to −1~1): energy + irradiation + daylight.

As found in Figure 12b, SA did not converge within this short-term search, showing the worst performance. A discrete search performed better. In Figure 10, we find building forms evolved to minimize glazing on the east and west and reduce energy loss and heat gain, while compromising daylight availability on the north and south. In this process, PS found an optimal solution rapidly, whereas MAPS converged at the vicinity of a local optimum. It should be noted that T-APSSA approximated a global optimum, although an initial solution was the poorest. The findings of these two tests show that T-APSSA solves MOBPO problems well, even within a limited iteration.

5. Application to a Design Experiment and Results

5.1. Development of a Cyber-Physical BPS Interface Using VPL

The effectiveness and flexibility of GH as a BPS/parametric design platform was identified by Shi and Yang [22]. Simulation of illuminance in GH was enabled with DIVA, a Radiance-based GH plug-in, and the sky model and radiance data of a weather file were customized according to on-site sensor (photoresistor) data.

5.2. Field Tests: Synchronized Data Transfer and Design Optimization

In most cases of optimal building design using BPS, design objectives and parameters of building models and simulation are deterministically predefined or assumed [25]. This gives rise to a lot of uncertainty in optimization, which may even end up with biased results. To compare a conventional deterministic design optimization with a dynamic process, a baseline model was established. Referring to the indoor environmental quality (IEQ) credit 8, option 1 of the Leadership in Energy and Environmental Design (LEED) building certification standard, the baseline was a static form of exterior shading used to satisfy a spatial daylight autonomy (sDA) of 50% at 300 lux with no less than 55% of an analyzed space, and an annual solar exposure of no more than 10% of a space that receives above l000 lux for 250 hours throughout a year.

A cyber-physical interface integrating Arduino microcontrollers, sensors, GH, and BPS was constructed and tested with a simple box shading model and developed for the dynamic adaptive optimization process (Figures 13 and 14). A microcontroller with transceivers (RF24L01 and ESP8266) and a photoresistor were installed on the outside of the test building. The sensors were positioned in the center of the courtyard so that reception of irradiance was not hindered by any ground obstacles or shadows during test hours (Figure 13b). Outdoor natural light levels were sent to a remote computer wirelessly and logged into a data file every 10 minutes. The design interface read sensor data and reconstructed a local weather file using the database. This approach enabled designers to collect actual on-site information for early-stage BPS, and to predict the performance of responsive designs more accurately in remote places where signal reception is available.

5.3. Design Case Studies for Algorithm Verification

5.3.1. Validation of Daylight Performance

T-APSSA was coded to perform both deterministic and dynamic optimal shading design, and optimization was executed on a system processor of Intel Core^{TM} i7-7700 CPU 3.6 GHz with 32.0 GB RAM. We chose a honeycomb shape for the design, as it is one of popular parametric design patterns for shading. Figure 15 shows a responsive surface module (600 × 600 mm) of the test design. The module shape was designed to increase/reduce façade fenestration by geometry parameters with control points and θ ($0° \leq \theta \leq 41.1°$) in the center. Figure 16 presents the results of an optimization processed on 13 March 2017. For this actual test, 10:00 a.m. was chosen as the starting time, because it was the hour that the test façade likely received the most direct sunlight at the site (Figure 13b). Comparing performances by algorithms (Figure 16a–d), we can see that T-APSSA found solutions more quickly than other algorithms. Figure 17a–f shows dynamic optimal parametric form specific to actual outdoor weather data. For sensor-triggered (actual data-based) optimization, daylight simulation and T-APSSA optimization ran with the geometry parameters at each ping from the RF24L01. As part of the sustainable campus plan of FIU, the target space was supposed to achieve the certification of LEED BD+C. Accordingly, optimal parameters were found that permitted the minimum illuminance in the space to be 300 lux (LEED IEQ credit option 2). These results show that dynamic adaptation creates various building skins, while deterministic solutions only allow a small portion of perforation in the façade. Figure 16 plots the optimization process for each algorithm, and Figure 17 visualizes the morphological variation of the optimal solutions. This demonstrates the robustness of T-APSSA,

which sufficiently terminated the optimal search within a ping interval, while the final façade form actively varied according to the external data transfer when indoor daylight levels were optimized at 300 lux.

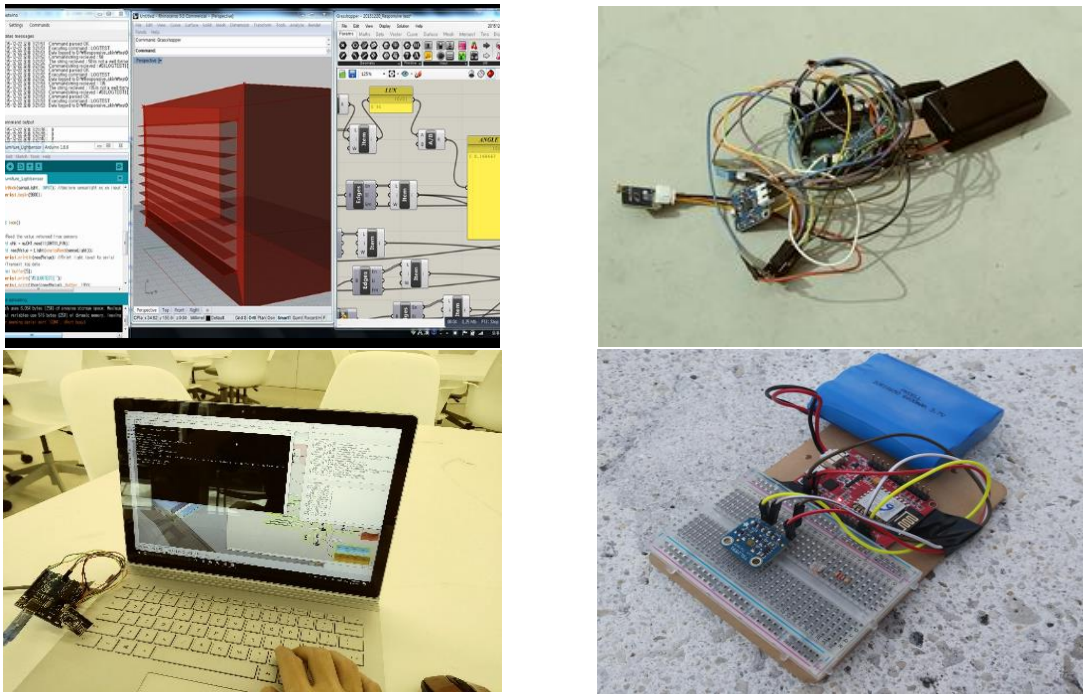

(**a**)

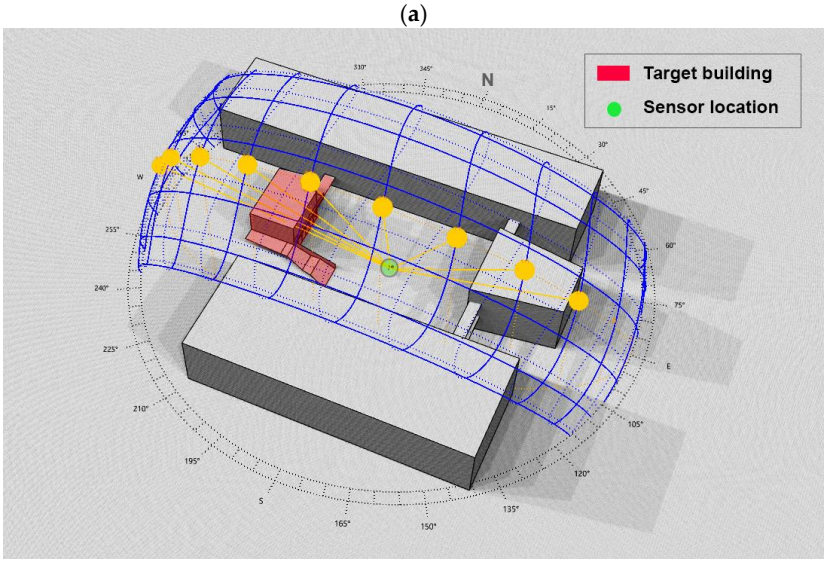

(**b**)

Figure 13. Interface integrated with remote sensor communication, BPS, and the parametric design process. (**a**) Installation work: interface, sensors, on-site Wi-Fi-IoT boards. (**b**) Shadow analysis and sensor installation (red point in the center): surrounding buildings do not cast shadows on the sensor from 9:00 a.m. to 3:00 p.m.

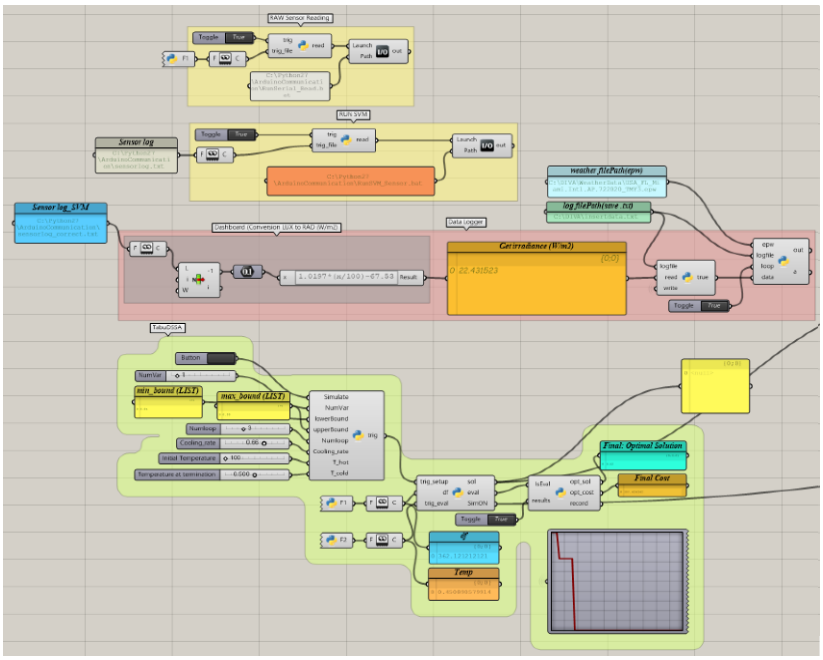

(**a**)

```
import serial, time
import sys

arduino = serial.Serial('COM4', 115200, timeout=1.5)
time.sleep(1)

arduino.flush()
while True:
    data = arduino.readlines()
    if data:
        target = data[0]
        target = target.decode("utf-8")
        target = target.replace('\n', '')
        f = open('C:/Python27/ArduinoCommunication/sensorlog.txt','w')
        f.write(target)
        f.close()
        time.sleep(2)
```

(**b**)

```
if trig_setup and sc.sticky["count_inital"] == 0:
    
    for i in range(sc.sticky["totalVarNum"]): sc.sticky["normal_solution"].append(random.random())    #get initial point
    sc.sticky["normal_solutionNew"] = sc.sticky["normal_solution"]
    #Record current sol&best in Tabu
    sc.sticky["listTabu_Var"].append(convSol(sc.sticky["normal_solution"]))
    sol = convSol(sc.sticky["normal_solution"])

if sc.sticky["T"] > sc.sticky["T_min"]:
    if df or trig_eval:
        
        if sc.sticky["count_newSol"] == True:
            
            sc.sticky["pollSize"] = math.sqrt(sc.sticky["meshSize"])   #MADS Polling (*pollSize)
            if sc.sticky["meshSize"] <= 1:
                sc.sticky["d"] = int(random.uniform(1, sc.sticky["pollSize"]/sc.sticky["meshSize"]))*sc.sticky["meshSize"]
            else: sc.sticky["d"] = sc.sticky["meshSize"]
            sc.sticky["meshVertices"] = getMesh(sc.sticky["normal_solutionNew"], sc.sticky["d"], sc.sticky["vecBasis"])

            #Check Tabu
            for vertex in sc.sticky["meshVertices"]:
                if convSol(vertex) in sc.sticky["listTabu_Var"]:
                    sc.sticky["meshVertices"].remove(vertex)
```

(**c**)

Figure 14. Design and optimization interface development. (**a**) User interface: GH component design. (**b**) Serial communication. (**c**) Part of T-APSSA scripts encoded in GH.

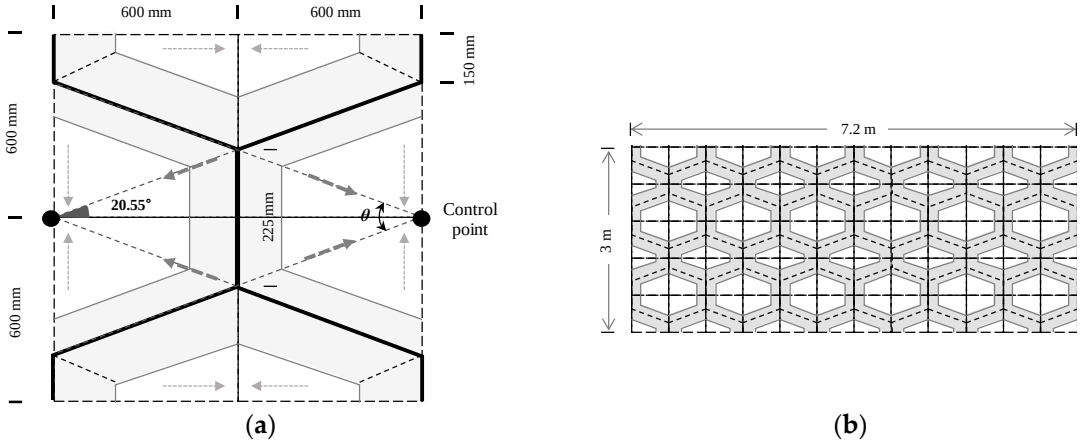

Figure 15. Test responsive surface module and combination over the test façade. (**a**) test façade module; (**b**) module combination over the test building surface.

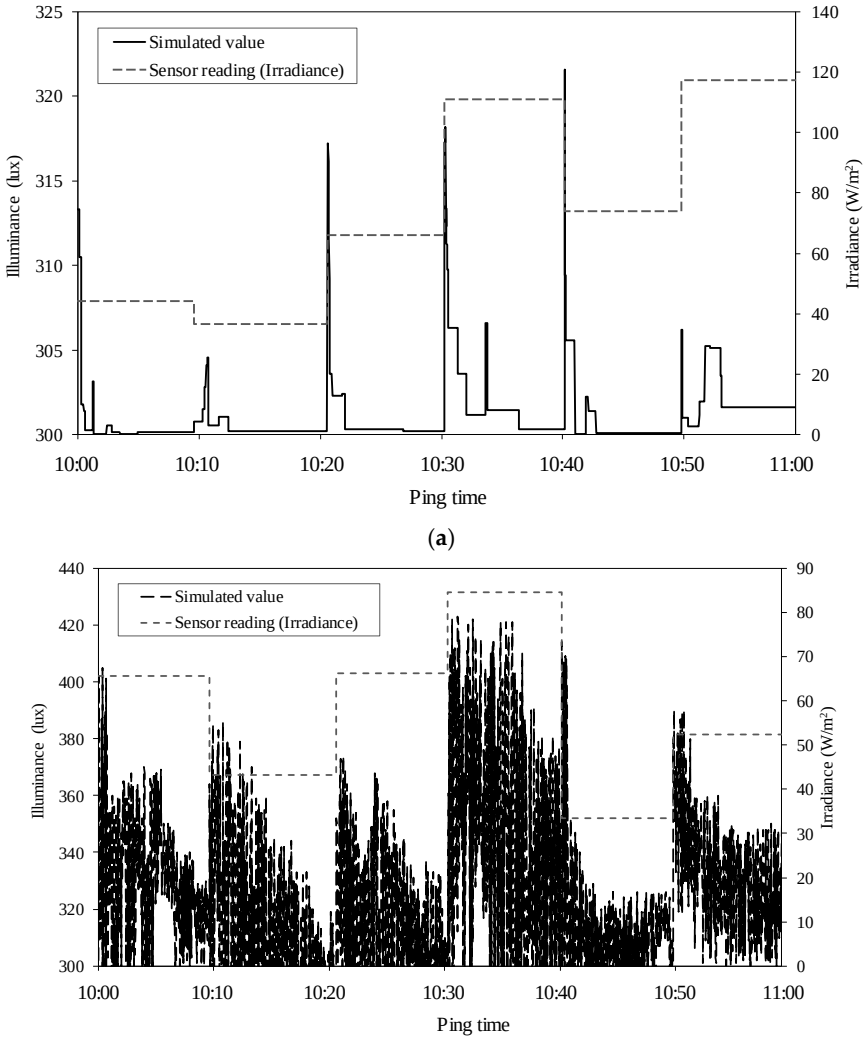

Figure 16. *Cont*.

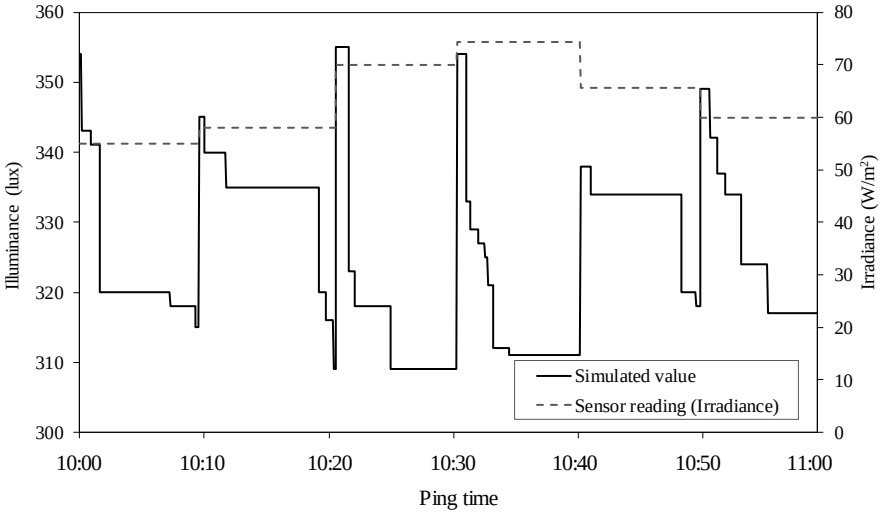

(**c**)

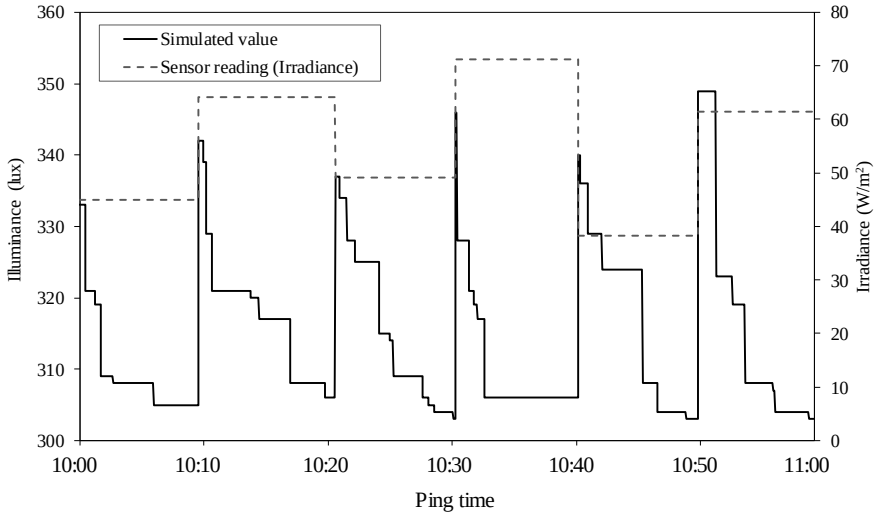

(**d**)

Figure 16. Results of optimization for daylight performance (13 March 2017). (**a**) T-APSSA; (**b**) SA; (**c**) PS; (**d**) MAPS.

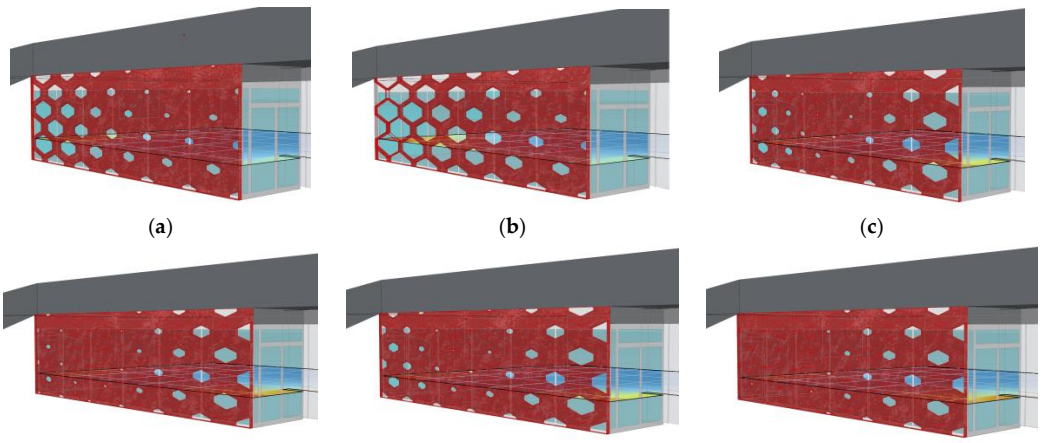

(**a**) (**b**) (**c**)

(**d**) (**e**) (**f**)

Figure 17. Optimal solutions for responsive shading motion (daylight). (**a**) 10:10 a.m. (13 March 2017). (**b**) 10:20 a.m. (13 March 2017). (**c**) 10:30 a.m. (13 March 2017). (**d**) 10:40 a.m. (13 March 2017). (**e**) 10:50 a.m. (13 March 2017). (**f**) 11:00 a.m. (13 March 2017).

5.3.2. Validation of Energy Performance and Multi-Objective Optimization

The performance of T-APSSA was further validated for energy and multi-objective BPS of two cases (minimizing cooling load and daylight, and minimizing lighting energy and cooling load, respectively). For the same design and test location, we executed T-APSSA optimization with Rhino GH VPL (Figure 14a) modified to carry out multi-objective optimization. In daylight simulation using radiance, an input weather parameter (irradiance) brought out a result at a specific time and location. However, energy simulation using EP requires a large set of premeasured annual weather data, and the hourly resolution of energy load calculation made it hard to take temporally changing on-site information while in simulation. Moreover, the performance of T-APSSA needs to be validated over a larger period of time before employing it for the long-term responses of building façades. For this reason, multi-objective T-APSSA was tested by setting specific simulations periods at the summer solstice (21 June) and over a year, rather than synchronizing on-site sensor data. Figures 18 and 19 exhibit iteration processes and optimal results. Each test was done with five trials to avoid biased finding. In the experiments, we found that, given the shading design, daily and annual cooling loads could be reduced up to 26.3 MJ and 10.2 GJ, respectively. Figure 18a,b shows how T-APSSA finds minimal values (starting temperature: 200 K; cooling rate: 0.8; termination: 0.5 K; number of mesh loops: 3). These results demonstrate that T-APSSA works with energy simulation at a very low starting temperature, compared with general SA; all cases were terminated before 100 iterations, and within only 40 iterations for the annual simulation (Figure 18b), taking an average time of 6 and 11 minutes, respectively. T-APSSA was applied to minimize both cooling energy and indoor illuminance (Figure 18c,d). For evaluation, two different simulation results were normalized to values between 0 and 1 by using the min–max scaling method. Despite the rapid search ability, Figure 18c,d shows that multi-objective T-APSSA undergoes a relatively more complex process with a longer termination time. By increasing the initial temperature to 20,000 K, T-APSSA searched for optima in 200~300 iterations. Hourly daylight simulation of Radiance was much slower than EP and became a primary cause of delayed searching. T-APSSA took 2 h 14 min and 3 h 43 min for termination for Figure 18c,d, respectively. To identify reasons for the sharp increase of elapsed time, we randomly generated 1000 solutions for each case. We found that the complexity of multi-objective T-APSSA was also influenced by the characteristics of a search domain. Figure 18e,d shows that a large number of points are cornered or concentrated in narrow areas, and Pareto curves included few points around optimal values. This finding suggests that the appropriate choice of cost-rescaling method, search parameters, and time window of simulation are important to get a better performance from T-APSSA.

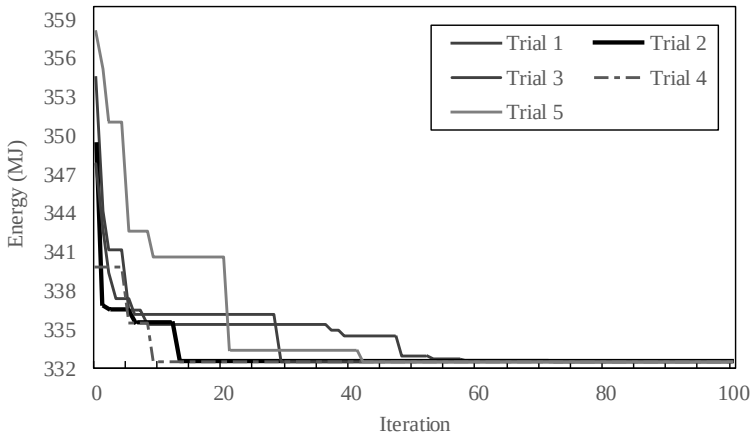

(**a**)

Figure 18. *Cont.*

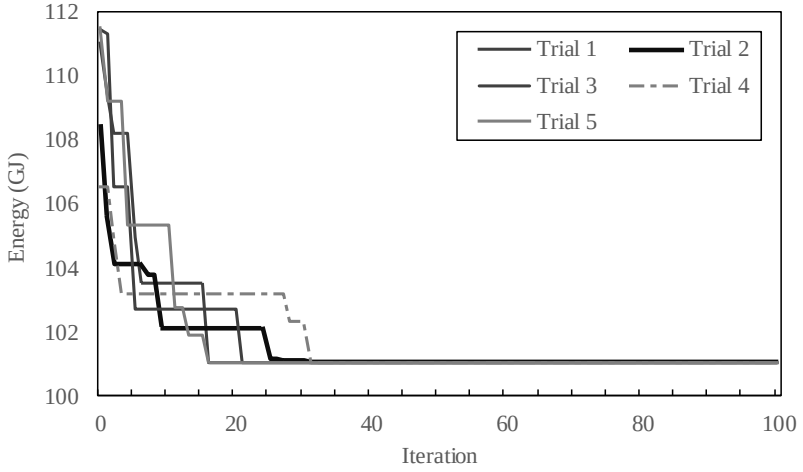

(**b**)

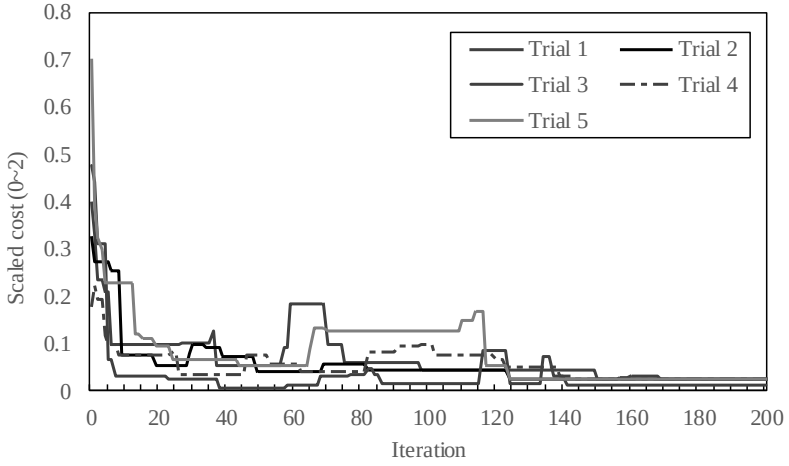

(**c**)

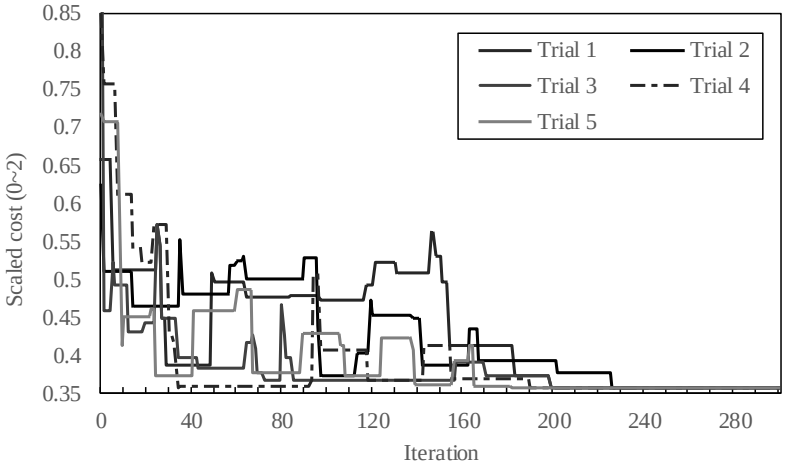

(**d**)

Figure 18. *Cont*.

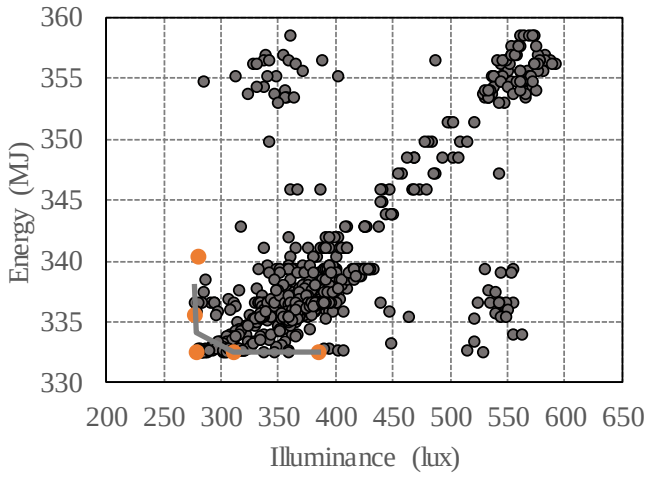

(**e**)

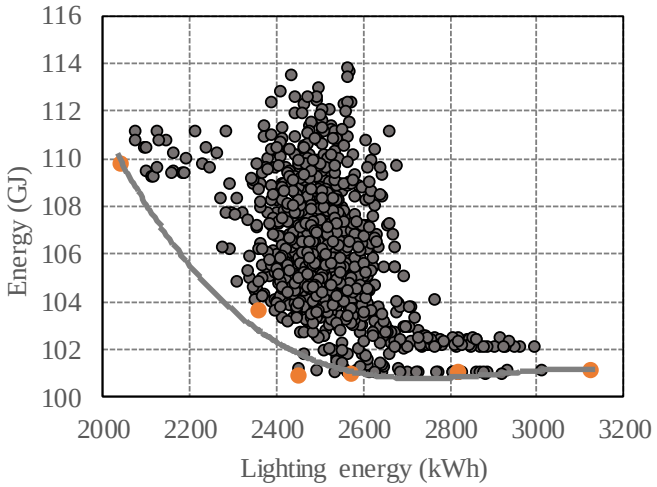

(**f**)

Figure 18. Results of optimization for daylight performance (energy and multi-objectives). (**a**) Cooling energy use (21 June 2017). (**b**) Annual cooling energy use. (**c**) Multi-objectives: cooling energy and illuminance (21 June 2017). (**d**) Multi-objectives: annual energy (cooling and lighting). (**e**) Pareto curve: multi-objectives (21 June 2017). (**f**) Pareto curve: multi-objectives (annual).

(**a**) (**b**)

Figure 19. *Cont*.

(**c**) (**d**)

Figure 19. Optimal solutions for responsive shading motion (energy and multi-objectives). (**a**) Cooling energy use (summer solstice). (**b**) Annual cooling energy use. (**c**) Multi-objectives: cooling energy and illuminance (21 June 2017). (**d**) Multi-objectives: annual energy (cooling and lighting).

6. Conclusions and Future Work

In the building industry, growing attention to geometrical responsiveness owes its adaptability in many ways to changes in surroundings and promises of sustainable and healthier built environments. The architectural practice is transforming toward smart and intelligent environmental building design and integrating BPS and optimization into the design process has become a major issue in finding better ways to assure the rapid feedback of decision-making. However, despite significant interest and advancements over the past few years, research on the performance-based design "process" to support responsive building is in its infancy. Indeed, although high performance responsive building design must be built upon the identification of controllable geometry (building envelope, in most cases) as well as the environmental effectiveness of responsive forms, and there is a dearth of strong practices in dynamic BPS and in the optimization of movable building forms during the early stages of building design. This study proposed a methodology for designers to quickly identify optimized variations of formal responsive patterns and performance of designs with remote sensor data measurements using a unified design platform. In practice, lagging optimization solutions for building design have been the most dominant barrier to the application of parametric digital tools for responsive building design. T-APSSA, a novel rapid optimization algorithm hybridizing tabu, SA, and direct search was suggested by taking a pragmatic approach to quicken the performance-based optimization of the dynamic forms of building surfaces. As observed in the algorithm test (Figure 12), T-APSSA outperformed the existing algorithms by far, taking advantage of the rapid convergence of local searching (PS) and the accuracy of global/constrained searching (SA and Tabu). The algorithm and wireless data communication integrated in the VPS-based parametric design software (Rhino) successfully supported streamlined geometric design, optimization, and simulation.

The experiments in this study presented a comparative study of design optimization algorithms with the suggestion of an advanced hybrid metaheuristics. For bi-directional parameter updates of BPS, physical remote data communication equipment was interfaced via a virtual parametric design tool. The application of the framework to the shading design process (Figure 15) indicates that a deterministic approach to design optimization with predefined simulation parameters is ill-suited to characterizing dynamic climatic adaptation in building design. Daylight simulation results also demonstrated that the formal responses of building façades benefit the comfort and sustainability of indoor spaces. It is now clearly understood that the combination of rapid optimization and sensor data communication with machine-learning prediction augments the sustainable building design process, making it far more suited to handling interactive forms and envisioning a potential of leveraging BPS to the design and control of building actuation systems. The developed framework can be used for virtual tests of the remote optimal controllability of the parametric design process, as well as the rapid prototyping of responsive building designs. In the method, we used a digital building model coupled with a physical data-transferring system, but the findings suggest that this integration

could be extended to involve physical scale models or mockups with sensor-simulation networking to characterize a variety of building performances, including energy use, human behavior, and so forth.

This understanding can be strengthened with various applications, yet this study is limited to elucidating a single building component (façade window), focusing only on interior illuminance. Accordingly, future studies need to follow up with further experiments that incorporate various types of sensor-captured data, co-simulation of lighting, energy use, indoor air-flow, algorithmic advancements to set dynamic parameters (annealing temperature and cooling rate of SA, TL size, etc.), and MOBPO with different forms of façade/shading design modules.

Author Contributions: H.Y. designed this study and developed the algorithm, managing overall work process. M.-J.K. and Y.K. conducted design experiments. S.-S.K. and K.-I.L. reviewed to verify research outcomes, collaborating to complete the manuscript with H.Y.

Funding: This work was supported by the National Research Foundation of Korea (NRF) grant funded by the Korea government (MEST) (NRF-2018R1C1B5084299).

Acknowledgments: The authors would like to thank colleagues in CARTA, Florida International University for their encouragements and supports.

Conflicts of Interest: The authors declare no conflict of interest.

Nomenclature

Ω	Solution domain
$\boldsymbol{x}^{\theta}$	Vector representing θ-th trial solution
$\boldsymbol{\Delta}_i$	Mesh size parameter of direct search
Δ^q	Poll size parameter of direct search
N_i	Mesh grid space
d_k	Spanning coordinate axis
E	Evaluation fitness
ξ	Tabu memory length
$\boldsymbol{t}$	Tabu list vector
r_{TR}	Radius of a circle around $\boldsymbol{t}$
λ	Random number

Appendix A

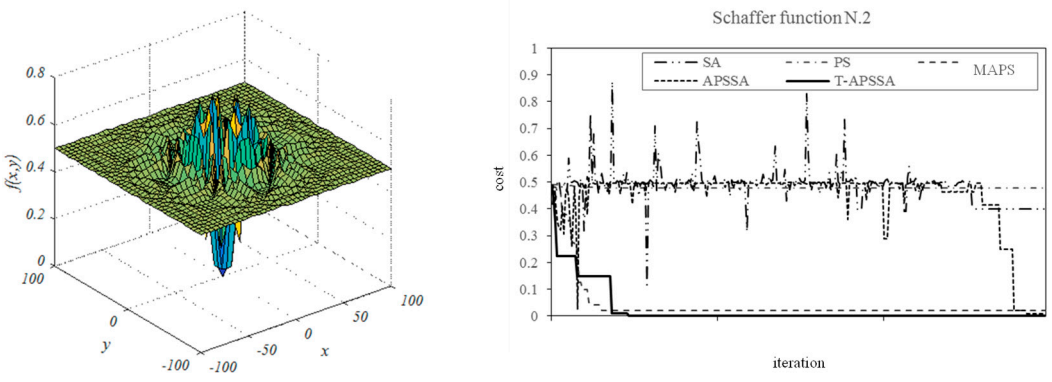

Schaffer function: $f(x,y) = 0.5 + \sin^2(x^2 - y^2) - 0.5/[1 + 0.001(x^2 + y^2)]^2$; $f_{min} = f(0,0) = 0$; $-100 \le x, y \le 100$

Figure A1. *Cont.*

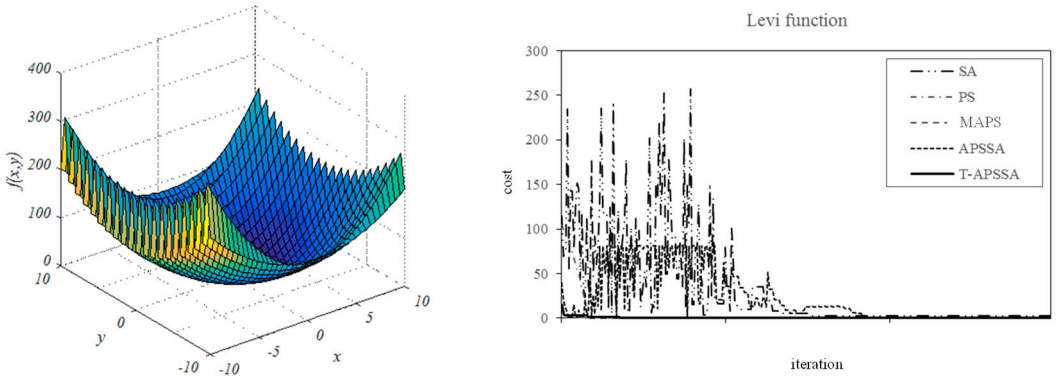

Lévi function N.13: $f(x,y) = \sin^2 3\pi x + (x-1)^2(1+\sin^2 3\pi y) + (y-1)^2(1+\sin^2 2\pi y)$; $f_{min} = f(1,1) = 0$, $-10 \le x, y \le 10$

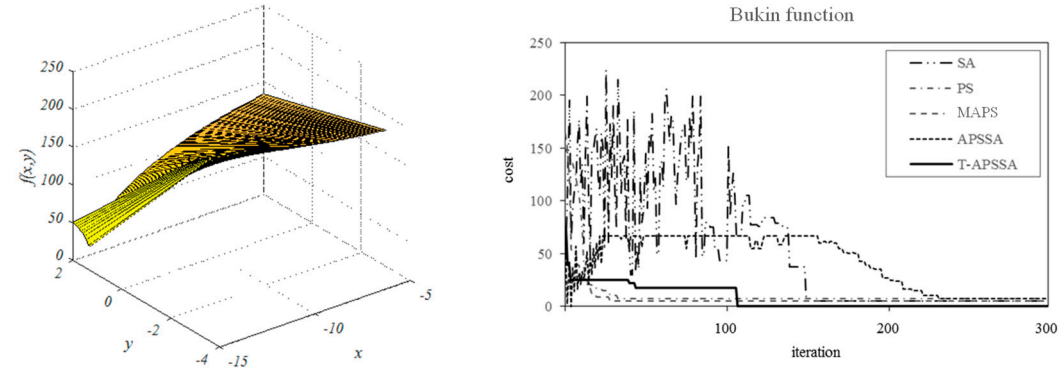

Bukin function: $f(x,y) = 100\sqrt{(|y - 0.01x^2|)} + 0.01|x + 10|$; $f_{min} = f(-10,1) = 0$; $-15 \le x \le -5$, $-3 \le y \le 3$

Figure A1. Additional validation of T-APSSA performance using test functions for optimization.

References

1. Kroner, W.M. An intelligent and responsive architecture. *Autom. Constr.* **1997**, *6*, 381–393. [CrossRef]
2. Sullivan, C.C. Robo buildings: Pursuing the interactive envelope. *Archit. Rec.* **2006**, *194*, 149–156.
3. Meagher, M. Designing for change: The poetic potential of responsive architecture. *Front. Archit. Rec.* **2015**, *4*, 159–165. [CrossRef]
4. Al Bahar Tower. Available online: https://en.wikiarquitectura.com/building/al-bahar-towers/ (accessed on 12 February 2017).
5. Lópeza, M.; Rubio, R.; Martín, S.; Croxford, B. How plants inspire façades. From plants to architecture: Biomimetic principles for the development of adaptive architectural envelopes. *Renew. Sustain. Energy Rev.* **2017**, *67*, 692–703. [CrossRef]
6. Torgal, F.P.; Labrincha, J.A.; Diamanti, M.V.; Yu, C.-P.; Lee, H.K. *Biotechnologies and Biomimetics for Civil Engineering*, 1st ed.; Springer: New York, NY, USA, 2015.
7. Henriques, G.C.; Duarte, J.P.; Leal, V. Strategies to control daylight in a responsive skylight system. *Autom. Constr.* **2012**, *28*, 91–105. [CrossRef]
8. Loonen, R.C.G.M. Bio-inspired Adaptive Building Skins. In *Biotechnologies and Biomimetics for Civil Engineering*; Torgal, F.P., Labrincha, J.A., Diamanti, M.V., Yu, C.-P., Lee, H.K., Eds.; Springer: New York, NY, USA, 2015; pp. 115–134.
9. Al-Obaidi, K.M.; Ismail, M.A.; Hussein, H.; Rahman, A.M.A. Biomimetic building skins: An adaptive approach. *Renew. Sustain. Energy Rev.* **2017**, *79*, 1472–1491. [CrossRef]
10. Ben bacha, C.; Bourbia, F. Effect of kinetic façades on energy efficiency in office buildings—Hot dry climates. In Proceedings of the 11th Conference on Advanced Building Skins, Bern, Switzerland, 10–11 October 2016; Available online: http://hdl.handle.net/1969.1/158209 (accessed on 21 March 2017).
11. Lee, D.-S.; Koo, S.-H.; Seong, Y.-B.; Jo, J.-H. Evaluating Thermal and Lighting Energy Performance of Shading Devices on Kinetic Façades. *Sustainability* **2016**, *8*, 883. [CrossRef]

12. Negendahl, K. Building performance simulation in the early design stage: An introduction to integrated dynamic tools. *Autom. Constr.* **2015**, *54*, 39–53. [CrossRef]
13. Macdonald, I.; Strachan, P. Practical application of uncertainty analysis. *Energy Build.* **2001**, *33*, 219–227. [CrossRef]
14. Yi, H. Automated generation of Optimized building envelope: Simulation based multi-objective process using Evolutionary algorithm. *Int. J. Sustain. Build. Technol. Urban Dev.* **2014**, *5*, 159–170. [CrossRef]
15. Johansson, C.; Evertsson, G. *Optimizing Genetic Algorithms for Time Critical Problems*; Department of Software Engineering and Computer Science, Blekinge Institute of Technology: Ronneby, Sweden, 2003.
16. Hyde, R. From biomimetic design to Nearly Zero Energy Building. *Archit. Sci. Rev.* **2015**, *58*, 103–105. [CrossRef]
17. Zuk, W.; Clark, R.H. *Kinetic Architecture*; Van Nostrand Reinhold: New York, NY, USA, 1970.
18. Yi, H. Robotics and kinetic design for underrepresented minority (URM) students in building education: Challenges and opportunities. *Comput. Appl. Eng. Educ.* **2018**, *27*, 351–370. [CrossRef]
19. Gruber, P.; Bruckner, D.; Hellmich, C.; Schmiedmayer, H.-B.; Stachelberger, H.; Gebeshuber, I.C. Biomimetics-Materials. In *Structures and Processes: Examples, Ideas and Case Studies*; Springer: New York, NY, USA, 2011.
20. Lin, S.E.; Gerber, D.J. Designing-in performance: A framework for evolutionary energy performance feedback in early stage design. *Autom. Constr.* **2014**, *38*, 59–73. [CrossRef]
21. Andia, A.; Spiegelhalter, T. *Post-Parametric Automation in Design and Construction*; Artech House: Boston, MA, USA, 2015.
22. Shi, X.; Yang, W. Performance-driven Architectural Design and Optimization Technique from a Perspective of Architects. *Autom. Constr.* **2013**, *32*, 125–135. [CrossRef]
23. Yi, H. User-driven Automation for Optimal Thermal zone Layout during Space Programming Phases. *Archit. Sci. Rev.* **2016**, *59*, 279–306. [CrossRef]
24. Mavromatidis, L. Coupling architectural synthesis to applied thermal engineering, constructal thermodynamics and fractal analysis: An original pedagogic method to incorporate "sustainability" into architectural education during the initial conceptual stages. *Sustain. Cities Soc.* **2018**, *39*, 689–707. [CrossRef]
25. Díaz, H.; Alarcón, L.F.; Mourgues, C.; García, S. Multidisciplinary Design Optimization through process integration in the AEC industry: Strategies and challenges. *Autom. Constr.* **2017**, *73*, 102–119. [CrossRef]
26. Nguyen, A.T.; Reiter, S.; Rigo, P. A review on simulation-based optimization methods applied to building performance analysis. *Appl. Energy* **2014**, *113*, 1043–1058. [CrossRef]
27. Anandalingam, G.; Friesz, T.L. Hierarchical optimization: An introduction. *Ann. Oper. Res.* **1992**, *34*, 1–11. [CrossRef]
28. Negendahl, K.; Nielsen, T.R. Building energy optimization in the early design stages: A simplified method. *Energy Build.* **2015**, *105*, 88–99. [CrossRef]
29. Yi, H.; Srinivasan, R.S.; Braham, W.W. An Integrated Energy-Emergy Approach to Building Form Optimization: Use of Energy Plus, Emergy Analysis and Taguchi-Regression Method. *Build. Environ.* **2015**, *84*, 89–104. [CrossRef]
30. Deb, K. *Multi-Objective Optimization Using Evolutionary Algorithms*, 1st ed.; John Wiley & Sons: New York, NY, USA; Chichester, UK, 2001.
31. Whitley, D. An overview of evolutionary algorithms: Practical issues and common pitfalls. *Inf. Softw. Technol.* **2001**, *43*, 817–831. [CrossRef]
32. van Laarhoven, P.J.; Aarts, E.H. *Simulated Annealing: Theory and Applications*; Kluwer Academic Publishers: Norwell, MA, USA, 1987.
33. Dolan, E.D.; Lewis, R.M.; Torczon, V.; Institute for Computer Applications in Science and Engineering. *On the Local Convergence of Pattern Search*; ICASE: Hampton, VA, USA; Hanover, MD, USA, 2000.
34. Audet, C.; Dennis, J.E., Jr. Mesh Adaptive Direct Search Algorithms for Constrained Optimization. *SIAM J. Optim.* **2006**, *17*, 188–217. [CrossRef]
35. Glover, F.; Marti, R. Tabu Search. In *Metaheuristic Procedures for Training Neutral Networks*; Alba, E., Marti, R., Eds.; Springer: New York, NY, USA, 2006.
36. Hedar, A.-R.; Fukushima, M. Tabu Search directed by direct search methods for nonlinear global optimization. *Eur. J. Oper. Res.* **2006**, *170*, 329–349. [CrossRef]

37. Arumí-Noe, F. Algorithm for the geometric construction of an optimum shading device. *Autom. Constr.* **1996**, *5*, 211–217. [CrossRef]
38. Futrell, B.J.; Ozelkan, E.C.; Brentrup, D. Optimizing complex building design for annual daylighting performance and evaluation of optimization algorithms. *Energy Build.* **2015**, *92*, 234–245. [CrossRef]
39. Fakra, A.H.; Boyer, H.; Miranville, F.; Bigot, D. A simple evaluation of global and diffuse luminous efficacy for all sky conditions in tropical and humid climate. *Renew. Energy* **2011**, *36*, 298–306. [CrossRef]